AGU PUBLICATIONS

JGR

Journal of Geophysical Research: Space Physics

RESEARCH ARTICLE
10.1002/2015JA021730

This article is a companion to *Stevenson and Parnell* [2015] doi:10.1002/2015JA021736.

Key Points:
- High-beta separator current layer reconnection has short fast and slow bursty phases
- Phase I strongest reconnection along the separator is away from nulls near flow counterrotation point
- Nature of magnetic field and velocity flow local to separator are correlated

Supporting Information:
- Movies S1–S3 captions
- Movie S1
- Movie S2
- Movie S3

Correspondence to:
J. E. H. Stevenson,
jm686@st-andrews.ac.uk

Citation:
Stevenson, J. E. H., and C. E. Parnell (2015), Spontaneous reconnection at a separator current layer: 1. Nature of the reconnection, *J. Geophys. Res. Space Physics*, *120*, 10,334–10,352, doi:10.1002/2015JA021730.

Received 28 JUL 2015
Accepted 12 NOV 2015
Accepted article online 13 NOV 2015
Published online 10 DEC 2015

Spontaneous reconnection at a separator current layer: 1. Nature of the reconnection

J. E. H. Stevenson[1] and C. E. Parnell[1]

[1]School of Mathematics and Statistics, Mathematical Institute, North Haugh, University of St. Andrews, St. Andrews, Scotland

Abstract Magnetic separators, which lie on the boundary between four topologically distinct flux domains, are prime locations in three-dimensional magnetic fields for reconnection, especially in the magnetosphere between the planetary and interplanetary magnetic fields and also in the solar atmosphere. Little is known about the details of separator reconnection, and so the aim of this paper, which is the first of two, is to study the properties of magnetic reconnection at a single separator. Three-dimensional, resistive magnetohydrodynamic numerical experiments are run to study separator reconnection starting from a magnetohydrostatic equilibrium which contains a twisted current layer along a single separator linking a pair of opposite-polarity null points. The resulting reconnection occurs in two phases. The first is short involving rapid reconnection in which the current at the separator is reduced by a factor of around 2.3. Most (75%) of the magnetic energy is converted during this phase, via Ohmic dissipation, directly into internal energy, with just 0.1% going into kinetic energy. During this phase the reconnection occurs along most of the separator away from its ends (the nulls) but in an asymmetric manner which changes both spatially and temporally over time. The second phase is much longer and involves slow impulsive bursty reconnection. Again, Ohmic heating dominates over viscous damping. Here the reconnection occurs in small localized bursts at random anywhere along the separator.

1. Introduction

Many highly energetic space physics processes involve magnetic reconnection, such as solar and stellar flares, coronal mass ejections, interactions between planetary and interplanetary magnetic fields, and substorms in magnetospheres. Two key papers that explained the basics of generalized three-dimensional (3-D) reconnection [*Schindler et al.*, 1988; *Hesse and Schindler*, 1988] provide the corner stones to all 3-D reconnection studies. In particular, one of their main results reveals that unlike 2-D reconnection, 3-D reconnection can occur either with or without null points.

In 3-D, reconnection has been shown to occur at a multitude of sites, such as at topological features including 3-D null points (locations where all three components of the magnetic field equal zero) [e.g., *Craig et al.*, 1995; *Pontin et al.*, 2004, 2005; *Pontin and Galsgaard*, 2007; *Priest and Pontin*, 2009; *Masson et al.*, 2009; *Pontin et al.*, 2011] and magnetic separators (special field lines that link pairs of 3-D null points) [e.g., *Priest and Titov*, 1996; *Longcope and Cowley*, 1996; *Longcope*, 2001; *Haynes et al.*, 2007; *Parnell et al.*, 2010a, 2010b; *Wilmot-Smith and Hornig*, 2011] or at the geometrical features known as quasi-separatrix layers (regions of magnetic field, which at one end are closely anchored but at the other end are anchored far apart) [e.g., *Priest and Démoulin*, 1995; *Demoulin et al.*, 1996, 1997; *Aulanier et al.*, 2005, 2006] and in twisted or braided flux tubes [e.g., *Galsgaard and Nordlund*, 1996, 1997a, 1997b; *De Moortel and Galsgaard*, 2006a, 2006b; *Wilmot-Smith and De Moortel*, 2007; *Browning et al.*, 2008; *Hood et al.*, 2009; *Bareford et al.*, 2013].

The reconnection that we focus on here is that associated with magnetic separators. Such reconnection has been invoked as an explanation for a number of specific observed solar flares [e.g., *Longcope et al.*, 2005; *Barnes et al.*, 2005], for flux emergence events [e.g., *Parnell et al.*, 2010b; *MacTaggart and Haynes*, 2014], and in the heating of the quiet Sun [e.g., *Close et al.*, 2004]. Furthermore, magnetic separators have been found to occur on a wide range of scales for they are found in global magnetic field extrapolations from photospheric synoptic magnetograms extending over several solar radii [e.g., *Platten et al.*, 2014; *Edwards et al.*, 2015] and also in local magnetic extrapolations of the quiet Sun from high-resolution magnetograms [e.g., *Close et al.*, 2005]. Additionally, magnetic reconnection plays an important role in planetary magnetospheres enabling the

interaction of the interplanetary and planetary magnetic fields and powering flux transfer events and substorms. Indeed, separators have been identified in numerous models of the Earth's magnetosphere [e.g., *Hu et al.*, 2004; *Laitinen et al.*, 2006, 2007; *Dorelli et al.*, 2007; *Dorelli and Bhattacharjee*, 2008, 2009; *Hu et al.*, 2009; *Pulkkinen et al.*, 2010; *Ouellette et al.*, 2010; *Peng et al.*, 2010; *Cnossen et al.*, 2012; *Komar et al.*, 2013]. Notably, *Komar et al.* [2013] have shown that on the dayside magnetopause, regardless of the direction of the interplanetary magnetic field (IMF), magnetic reconnection is most likely to occur at separators.

There are only limited "observations" of magnetic separators in the Earth's magnetosphere. This is not surprising since, as pointed out by *Parnell et al.* [2010a], "for 3D magnetic fields, global 3D topological structures and local 3D field structures do not [necessarily] coincide." Since separators are global structures, this means that it is difficult to determine separators unless the magnetic field is known "practically everywhere, which is obviously not the case from solar and magnetospheric observations." Nonetheless, published results claiming to have detected reconnection at separators using Cluster data include the work of *Phan et al.* [2006] who reported an observed separator (called, in their paper, an X line) on the Earth's dayside, while *Xiao et al.* [2007] report having observed separator reconnection in the nightside magnetosphere. *Deng et al.* [2009] and *Guo et al.* [2013] also report examples of separator reconnection observed using Cluster data.

We note that in some of the works referenced here, the term "X line" is used in place of "magnetic separator" since it is thought that the projected magnetic field in a plane perpendicular to a 3-D magnetic separator is X type and looks like a 2-D null point. This is not true since in 3-D the global topology and local magnetic field are not necessarily coincident as they are in 2-D. So although the projection of the global topology in a plane perpendicular to a separator is X type, the projection of the local magnetic field in such a plane may be X type or O type [*Parnell et al.*, 2010a]. Further to this, the term X line is often used to describe a line of nulls, which is an unstable feature [*Hesse and Schindler*, 1988] and entirely different from a magnetic separator. A 3-D magnetic separator may be regarded as a 2.5-D X line (a 2-D null point with a guide field).

A separator is a special field line that connects a positive null to a negative null (separators may also connect two bald patches or a null and a bald patch [see, for example, *Titov et al.*, 1993; *Haynes*, 2008], but we do not concern ourselves with such separators here). A positive/negative 3-D null is associated with a pair of spine lines (field lines which are directed into/away from the null point) and a separatrix surface (a surface of field lines pointing away from/into the null point). A separator is formed when (i) the separatrix surfaces of two oppositely signed nulls intersect, (ii) the spine of one null point intersects with the separatrix surface of another null point of the same sign, and (iii) the spines of two oppositely signed nulls intersect. Item (i) is the only one which is both general and generic since the others are unstable to perturbations (i.e., small perturbations would cause them to disappear resulting in a change to the structure of the topology of the magnetic field) and, hence, is the only type considered in this paper. A separator lies on the boundary of four topologically distinct flux domains (i.e., movement between the domains would result in a discontinuous jump in field line mapping), and so field lines in the vicinity of separators are sensitive to flows across these boundaries. Hence, currents build easily along separators [*Lau and Finn*, 1990; *Haynes et al.*, 2007; *Parnell et al.*, 2010a, 2010b; *Stevenson et al.*, 2015], and so they are prime locations where 3-D reconnection occurs.

Separator reconnection has been studied both analytically and numerically [*Sonnerup*, 1979; *Lau and Finn*, 1990; *Longcope and Cowley*, 1996; *Galsgaard and Nordlund*, 1997b; *Galsgaard et al.*, 2000; *Longcope*, 2001; *Pontin and Craig*, 2006; *Haynes et al.*, 2007; *Dorelli and Bhattacharjee*, 2008; *Parnell et al.*, 2008, 2010a, 2010b; *Komar et al.*, 2013]. Reconnection at separators is known to be different from 3-D null point reconnection. In particular, *Parnell et al.* [2010a] studied the dynamic nature of separator reconnection in a model where two nulls, positioned on the base of the box, were moved together via boundary driving such that their separatrix surfaces intersected to form separators. They found that the parallel electric field along a separator varies spatially and temporally and may be multiply peaked, implying that there can be one or more local "hot spots" of reconnection along a separator. Additionally, these reconnection hot spots, which coincided with counter-rotating flows, occur away from the ends of the separator making separator reconnection distinct from 3-D null point reconnection. They discussed that the projected magnetic field in planes perpendicular to a separator may either be X type or O type, with, in their model, the X-type projected field regions corresponding to O-type flow and weaker reconnection and the O-type projected field regions corresponding to X-type flow and stronger reconnection. This finding has been questioned by some who believed that the twisted nature of the field was a result of the specific driving in the experiment.

In this work, we detail the properties of 3-D separator reconnection in a nondriven experiment, to avoid any such problems, and also where the null points and separator are far from the boundary. The model starts from a MHS equilibrium, containing a separator current layer and excess energy above that of a potential field, formed through the nonresistive relaxation of an initially nonpotential, non–force-free field, discussed in detail in *Stevenson et al.* [2015]. Reconnection is triggered at the separator current layer using an anomalous diffusivity to mimic the onset of microinstabilities. In nature it is believed that the slow driving of complex magnetic fields leads to equilibria forming which have current layers located, for instance, where the field line mapping is discontinuous. Reconnection can occur at such current layers via microinstabilities once the length scales are sufficiently short such that the magnetic Reynolds number, $R_m \leq 1$.

This approach is different to many works, which start from potential (minimum energy) fields that are driven on the boundaries (at slow or fast rates) to induce reconnection. In these situations, the resulting reconnection rate is typically found to depend on the rate of driving [e.g., *Galsgaard and Parnell*, 2005] and the nature of the initial magnetic configuration.

The approach we use has been used before to investigate reconnection at 2-D magnetic null points [e.g., *Fuentes-Fernández et al.*, 2012a, 2012b] where high and low plasma beta reconnection regimes were studied, respectively. The high- and low-beta MHS configurations, from which the reconnection experiments start, involve enhanced current not just at the null point, where it forms a null current layer, but also along the separatrices of the null. Everywhere else the current is very low. In contrast to *Longcope and Priest* [2007] and *Longcope and Tarr* [2012], (zero-beta models), the numerical models of *Fuentes-Fernández et al.* [2012a] (high beta) and *Fuentes-Fernández et al.* [2012b] (low beta) find that the reconnection process converted most of the magnetic energy (stored in the 2-D null current layer configuration) directly into internal energy, via Ohmic dissipation, with only a little being converted initially into kinetic energy and then damped due to viscosity. Additionally, *Fuentes-Fernández et al.* [2012a] found that the value of the magnetic diffusivity affects not only the reconnection rate but also the amount of magnetic energy converted into kinetic and internal energy.

All experiments studied here start with equilibria involving a separator current layer embedded in a high-beta plasma (detailed in *Stevenson et al.* [2015]). The so-called cluster separators (separators that link nulls clustered within a single weak field region [*Parnell et al.*, 2010b]) are likely to be in a high-beta plasma. These separators are typically short (approximately 1–2 Mm in length) [*Parnell et al.*, 2010b]. The vast majority of null points in the solar atmosphere occur low down [e.g., *Régnier et al.*, 2008; *Longcope and Parnell*, 2009; *Edwards and Parnell*, 2015] and thus will reside in the high-beta chromospheric region of the Sun; intercluster separators (linking nulls from different null clusters) that lie within the chromosphere are likely to have lengths below 10 Mm (considering the typical size of small-scale photospheric magnetic features). The plasma beta in the magnetosphere lies between 1 and 10 [*Trenchi et al.*, 2008]; thus, separator reconnection here is also likely to occur in a high-beta plasma. The lengths of these separators have been found to be greater than 200 Mm [*Komar et al.*, 2013; *Komar*, 2015]. As a result of this wide range of separator lengths, the results that we present here are nondimensional. We explain the appropriate scalings that should be applied to produce dimensional results applicable to the many varied space physics situations where reconnection occurs.

Here we study the nature of nondriven 3-D separator reconnection at a generic single-separator current layer. Specifically, we choose an idealistic setup (a straight single separator) to allow us to relatively easily analyze (i) the nature of the reconnection found at all points along the separator and (ii) the nature of the waves and flows [*Stevenson and Parnell*, 2015] resulting from the reconnection. In particular, we do not attempt to simulate one specific space physics event but rather produce a model whose general results may be applicable in many events involving separators. We look to answer the following: what is the partitioning of the magnetic energy released by the reconnection? And how is the reconnection rate affected by the value of the diffusivity, the size of the diffusion region, and the background viscosity? We compare our results to those of *Parnell et al.* [2010a], e.g., is the reconnecting magnetic field elliptic (helical) or hyperbolic? To what extent do the null points play a role in separator reconnection? And does reconnection occur along the entire length of the separator?

In section 2 we detail the properties of the MHS equilibrium and the current layer it contains. The numerical model used to carry out the experiments is discussed in section 3, followed by an analysis of the energetics of the main experiment (section 4). We then examine the nature of the reconnection (section 5) by analyzing where the reconnection is strongest and the plasma properties there. Finally, we detail the effects of varying

the diffusivity, the size of the diffusion region, and the background viscosity in the system (section 6) before summarizing our results (section 7).

2. MHS Equilibrium Current Layer

The MHS equilibrium used as the initial condition for our numerical experiments was formed through non-resistive MHD relaxation [*Stevenson et al.*, 2015]. The initial equilibrium is identical to that found by *Stevenson et al.* [2015] with the exception of an increased domain length in the z direction, but the grid resolution is the same. The dimensions of the numerical domain, in Cartesian coordinates, are $-1.0 \leq x, y \leq 1.0$ and $-1.75 \leq z \leq 2.75$ and in grid cells $(512, 512, 768)$.

The MHS equilibrium contains two 3-D null points located at $(0, 0, -0.10)$ and $(0, 0, 1.08)$ with a separator along the z axis linking them created from the intersection of their separatrix surfaces. (The null points in our model were tracked using the trilinear null finding method of *Haynes and Parnell* [2007], and the magnetic skeleton was found using the method described in *Haynes and Parnell* [2010].) This equilibrium contains a twisted current layer which lies along the separator. (Movie S1 shows a 360° view of the magnetic skeleton with the current layer shown in Figure 1a.) The dominant component of current in the current layer is parallel to the separator. Figure 1b shows a horizontal cut perpendicular to the separator at $z = 0.4$ (the location of the peak current along the separator) in which the strong current at the separator (pink contour) and along the separatrix surfaces (cyan curved contours) is visible. In this cut, an insert of the current layer around the separator is included to indicate its width, w, and depth, d. We have also plotted a yellow contour at $j_{\text{crit}} = 10$: the current above which the diffusivity is nonzero (see section 3).

In the MHS equilibrium, the separatrix surfaces that create the separator are twisted about it forming cusp regions in planes perpendicular to the separator. Within these cusps the plasma pressure is enhanced, and outwith them the plasma pressure is diminished. The equilibrium is not perfect: an infinite time would be required to achieve such a thing [*Stevenson et al.*, 2015]. Instead, very small localized residual pressure and Lorentz forces remain on the edge of the current layer about the separator and the separatrix surfaces near the separator. Outside the current layer the current is small and the field is in force balance.

3. Numerical Model

The MHS equilibrium current layer has length l_{sep}=1.18, depth $d = 0.06$, and width $w = 0.24$ (the latter two dimensions are calculated at $z = 0.4$). To study the reconnection that can occur at this separator current layer due to microinstabilities (modeled by introducing an anomalous diffusivity), we employ the 3-D resistive MHD code Lare3d [*Arber et al.*, 2001].

Lare3d solves the MHD equations in a frame that moves with the fluid and then maps the resulting Lagrangian grid geometrically back onto the original Eulerian grid. It uses a staggered grid in which the pressure (p), internal energy per unit mass (ϵ), and the density (ρ) are defined at the cell centers. The magnetic field components (B_x, B_y, B_z) are defined on the cell faces with the *Evans and Hawley* [1988] constrained transport method for magnetic flux employed to help maintain the solenoidal constraint, $\nabla \cdot \mathbf{B} = 0$. The velocity components (v_x, v_y, v_z) are defined on the cell vertices to prevent the checkerboard instability. The following normalized quantities (identified by the hats) represent dimensionless variables used by the code,

$$\mathbf{x} = L_n \hat{\mathbf{x}}, \qquad \mathbf{B} = B_n \hat{\mathbf{B}} \qquad \text{and} \qquad \rho = \rho_n \hat{\rho}, \tag{1}$$

where $\mathbf{x} = (x, y, z)$ is the position vector with L_n, B_n, and ρ_n representing the normalized length, magnetic field, and density, respectively. Using these normalizing factors, the normalising constants for the velocity, pressure, current, internal energy per unit mass, and plasma beta may be written, respectively, as

$$v_n = \frac{B_n}{\sqrt{\mu_0 \rho_n}}, \quad p_n = \frac{B_n^2}{\mu_0}, \quad j_n = \frac{B_n}{\mu_0 L_n},$$

$$\epsilon_n = v_n^2 = \frac{B_n^2}{\mu_0 \rho_n} \quad \text{and} \quad \beta = \frac{2\hat{p}}{\hat{B}^2}. \tag{2}$$

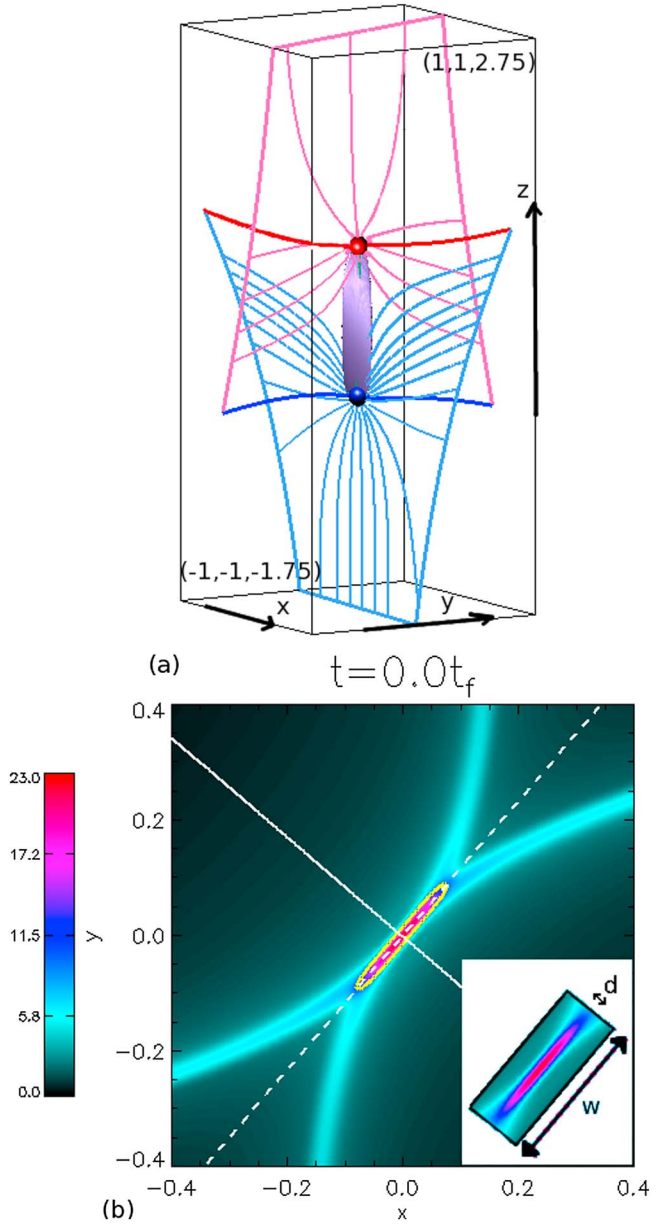

Figure 1. (a) Skeleton of the MHS equilibrium magnetic field with purple isosurface of $j_{\|} = 10.0$. Also shown are the positive/negative nulls (blue/red spheres) with associated spines (blue/red lines) and separatrix surface field lines (pale blue/pink lines) and the separator (green line, hidden by the current layer). The solid pale blue/pink lines indicate where the separatrix surfaces intersect the boundaries. Movie S1 shows a 360° view of Figure 1a. (b) Perpendicular cut across the MHS equilibrium separator at $z = 0.4$ showing contours of $|\mathbf{j}|$ and white solid/dashed lines going through the depth/across the width of the current layer, respectively. A yellow contour is drawn at $j_{crit} = 10$. The inserted image highlights the depth (d) and width (w) of the current layer in this plane.

Note in the code's dimensionless units the magnetic permeability $\mu_0 = 1$. This leads to the following resistive normalized MHD equations which are used in Lare3d (note that the hats have been dropped for simplicity)

$$\frac{D\rho}{Dt} = -\rho\nabla\cdot\mathbf{v}, \tag{3}$$

$$\frac{D\mathbf{v}}{Dt} = \frac{1}{\rho}(\nabla\times\mathbf{B})\times\mathbf{B} - \frac{1}{\rho}\nabla p + \frac{1}{\rho}\mathbf{F}_v, \tag{4}$$

$$\frac{D\mathbf{B}}{Dt} = (\mathbf{B}\cdot\nabla)\mathbf{v} - \mathbf{B}(\nabla\cdot\mathbf{v}) - \nabla\times(\eta\nabla\times\mathbf{B}), \tag{5}$$

$$\frac{\mathrm{D}\epsilon}{\mathrm{D}t} = -\frac{p}{\rho}\nabla\cdot\mathbf{v} + \frac{1}{\rho}H_\nu + \frac{j^2}{\rho\sigma}, \tag{6}$$

where t is time, $\mathbf{F}_\nu = \nu(\nabla^2\mathbf{v} + \frac{1}{3}\nabla(\nabla\cdot\mathbf{v}))$ is the viscous force (where ν is the background viscosity), $\eta = \mathbf{1}/(\mu_0\sigma)$ is the magnetic diffusivity where σ is the electric conductivity, $H_\nu = \nu(\frac{1}{2}e_{ij}e_{ij} - \frac{2}{3}(\nabla\cdot\mathbf{v})^2)$ is the viscous heating term (where e_{ij}, the rate of strain tensor, equals $(\partial v_i/\partial x_j)+(\partial v_j/\partial x_i)$), and σ is the electric conductivity. The term j^2/σ represents Ohmic dissipation, and our closure equation is $\epsilon = p/\rho(\gamma - 1)$ where γ, the ratio of specific heats, equals 5/3. The value of the background viscosity is $\nu = 0.01$. The background viscosity (which is equal to $\rho\nu_k$ where ν_k is the kinematic viscosity) plays a role in the viscous force, F_ν, and viscous heating terms, H_ν, discussed previously.

All times in this paper are normalized with respect to t_f, the time it would take a fast magnetoacoustic wave to travel from the lower null to the upper null along the path of the separator (z axis) in the initial MHS equilibrium:

$$t_f = \int_{z_l}^{z_u} \frac{1}{\sqrt{c_s(z)^2 + c_A^2(z)}}\mathrm{d}z = 0.88, \tag{7}$$

where $(0, 0, z_l)$ and $(0, 0, z_u)$ are the equilibrium positions of the lower and upper nulls respectively and $c_s(z)$ and $c_A(z)$ are the sound speed and the Alfvén speed at $(0, 0, z)$, respectively.

We employ line-tied boundary conditions to prevent energy leaving or entering the domain. Hence, the derivatives of the internal energy per unit mass and the density and all the components of the magnetic field normal to the boundaries are set to zero. The velocity is also set to zero on the boundaries ($\mathbf{v} = \mathbf{0}$).

To gain reconnection, resistive terms are included in the governing equations. We choose to use a nonuniform diffusivity which is zero unless the current is greater than a set amount, j_{crit},

$$\eta = \begin{cases} 0 & |\mathbf{j}| < j_{\mathrm{crit}}, \\ \eta_d & |\mathbf{j}| \geq j_{\mathrm{crit}}. \end{cases}$$

In our main experiment $j_{\mathrm{crit}} = 10$ such that diffusion only occurs at the separator current layer (and not on the current on the separatrix surfaces), $\eta_d = 0.001$, corresponding to an average R_m of 10^3 along the separator, and $\nu = 0.01$. An analysis of how varying η_d, j_{crit}, and ν effect the reconnection rate and the energy conversion is presented in section 6. The behavior in all our experiments is very similar, so we mainly concentrate on one (the main) experiment in order to describe the basic behavior that is seen in all experiments.

The initial setup for all experiments discussed in this paper is a MHS equilibrium. When we apply a nonzero diffusivity, reconnection occurs immediately (as will be discussed in detail in section 4). If $\eta_d = 0$, then the current layer in the equilibrium does not decay [see *Stevenson et al.*, 2015], indicating that the numerical diffusion is smaller than our range of values for η_d.

In the following sections, we describe the basic energetic behavior and partitioning found in the main experiment (section 4). Then the nature of the reconnection and magnetic field evolution are studied in section 5, while section 6 studies the effects of varying the diffusivity, the size of the diffusion region, and the background viscosity on the energetics and reconnection rate. Finally, in section 7, the conclusions are presented.

4. Energetics

In order to determine the response of the MHS equilibrium to the introduction of an anomalous diffusivity, we consider the system's energetics. The change in energies against time for the main resistive 3-D MHD experiment with η_d=0.001, j_{crit}=10, and ν=0.01 are plotted in Figure 2a, where the magnetic, internal, and kinetic energies are normalized to the maximum change in magnetic energy and the normalized kinetic energy is multiplied by 50 for representational purposes. Note that time is plotted on a logarithmic scale.

Since there is no Poynting flux on the boundaries (i.e., no gain or loss of energy through the boundaries), the change in total energy (ΔE_T) should be zero throughout the experiment. We find that it is zero to within a relative error of 2.1×10^{-5}%, indicating that the code properly conserves energy. Figure 2a shows that in the

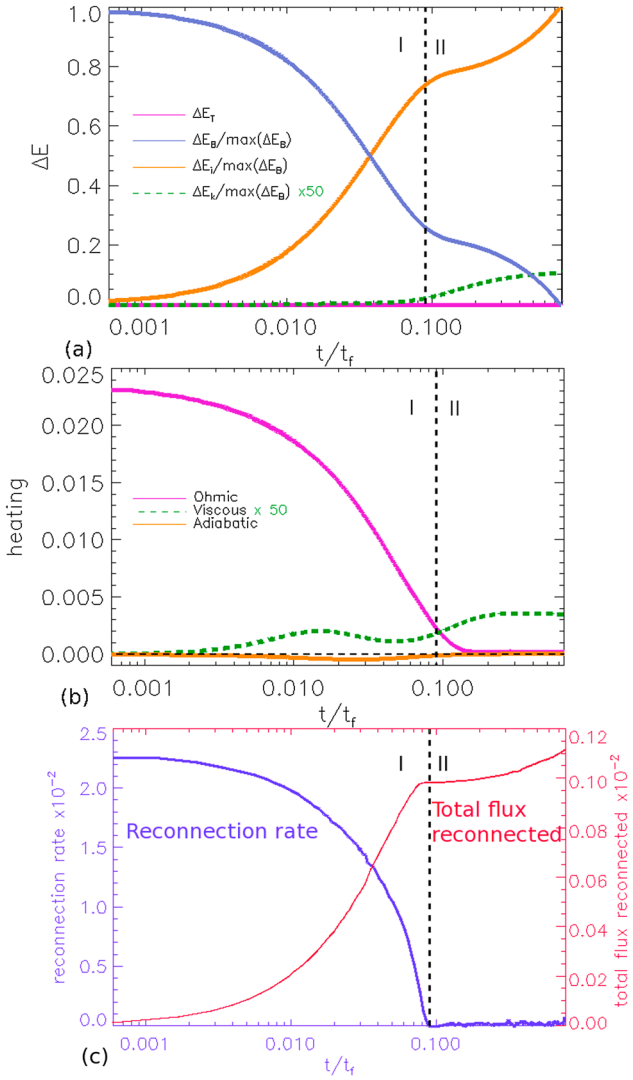

Figure 2. Plots of (a) the change in energies, (b) the instantaneous heating terms, and (c) the reconnection rate (blue line) and total flux reconnected (pink line). Note that the kinetic energy and viscous heating curves have been multiplied by 50 and both curves in Figure 2c have been multiplied by 100. The black dashed vertical lines highlight where the first phase ends (along with the symbols I and II) and the dashed horizontal line in Figure 2b indicates where zero lies.

first $0.09t_f$ of the experiment, magnetic energy (ΔE_B) is converted directly into internal energy (ΔE_I) with only a little going into kinetic energy (ΔE_K). During this time three quarters of the total loss in magnetic energy occurs. As seen from Figure 2b, this magnetic energy is converted into internal energy via Ohmic dissipation with only 0.23% going into kinetic energy.

Figure 2c shows the reconnection rate and the total flux reconnected during the experiment (calculated from $\int_l E_\parallel dl$ along the separator as in *Parnell et al.* [2010a], an approach that is validated by Figure 5). Clearly, the rate of reconnection before $t = 0.09t_f$ is dramatically different to that after, and so we define this time as the change between two different phases: phase I, the fast-reconnection phase (88% of the final total reconnected flux is reconnected here), and phase II, the slow impulsive bursty reconnection phase. Negligible reconnection occurs in the first few moments of the second phase (cf. the flat gradient just after $t = 0.09t_f$), but then small amounts of reconnection occur in bursts throughout the second phase. The vertical black dashed line on all these plots denotes where the change of phase occurs.

The existence of two distinct reconnection phases is not unexpected since the 2-D spontaneous reconnection experiments of *Fuentes-Fernández et al.* [2012a] and *Fuentes-Fernández et al.* [2012b] found the same behavior.

Fuentes-Fernández et al. [2012a] (high beta) found that the fast-reconnection phase was followed by a steady phase, as opposed to the bursty, reconnection phase we find. In their low-beta model a bursty reconnection phase was found, suggesting that one of the key differences between low- and high-beta spontaneous reconnection would be a much stronger impulsive bursty reconnection phase after the initial fast-reconnection phase.

Differences between the energetics of the two phases are evident in all graphs in Figure 2. During phase I, in addition to the reconnection, which begins at a high rate, but decreases rapidly so it is small by the end of the first phase, there is a minimal contribution from the viscous heating term (whose peak during this phase is just (1/500) of the peak Ohmic heating rate). A small amount of adiabatic cooling is also observed (Figure 2b) indicating that locally, a rapid expansion has occurred within the system.

As the first phase (in which there is fast Ohmic dissipation) comes to an end at $t=0.09t_f$, the gradients of the magnetic and internal energies change and the Ohmic heating rate decreases: most of the current above j_{crit} in the separator current layer has been dissipated. In phase II, the kinetic energy, which until now has been slowly building, increases sharply associated with the presence of flows in the system following the rapid adiabatic cooling (see *Stevenson and Parnell* [2015] for further details of the waves and flows created by this reconnection). This increase in kinetic energy is reflected by an increase in viscous heating to 8×10^{-5}; however, the amount of Ohmic heating is always greater than the viscous heating throughout both phases due to the high value of the plasma beta (the mean value of the plasma beta is $\bar{\beta}=4.8$ at $t=0t_f$) which makes it hard for large waves to be produced. In Figure 2b, the viscous heating has been multiplied by 50, which is why, in this plot, the viscous heating appears to be greater than the Ohmic heating in phase II. The kinetic energy and viscous heating terms level out toward the end of the experiment indicating that a phase of slow reconnection has started.

The reconnection in this experiment, therefore, occurs in two phases: the first phase is a highly dynamic fast-reconnection phase with low velocities which is dominated by Ohmic heating ($0t_f \leq t \leq 0.09t_f$) and the second phase is a slow impulsive bursty reconnection phase which has a comparatively low level of Ohmic heating, but with higher velocities than in phase I providing greater amounts of viscous heating ($0.09t_f < t \leq 0.76t_f$ where $t=0.76t_f$ is where we stop the experiment since at this time the waves, launched by the reconnection, approach the boundaries of the domain; see *Stevenson and Parnell* [2015] for more details).

In this paper, we focus on the properties of the reconnection in both phases of the experiments. In a follow-up paper we will detail the properties of the waves which travel out from the diffusion site, due to the sudden lack of force balance, and set up flows in the system.

5. Nature of the Reconnection

5.1. Magnetic Field Evolution

Reconnection at a 3-D magnetic separator is found to have several similar characteristics to 2-D null point reconnection (such as the flux from one pair of oppositely situated flux domains is transferred into another pair of oppositely situated flux domains). Figure 3 displays the nulls, their spines, the separator, and the same sample field lines (drawn initially in the two flux domains outwith the cusp regions, i.e., D_1 and D_2, respectively) at four times throughout the fast-reconnection phase, which lasts up until $t = 0.09t_f$. The earliest two times are plotted from both side and top views to show which domains the field lines lie in before and after the reconnection occurs. In these plots, field lines which have not reconnected are drawn as black and grey lines, if they lie in domains D_1 and D_2, respectively. Once reconnected, these field lines are colored orange and grey and lie in domains D_3 and D_4, respectively. This reconnection is not undertaken by a pairwise matching of field lines but by continual reconnection of field lines during their passage through the diffusion region.

As shown in Figure 2, and confirmed in Figure 3, much of the reconnection occurs within the first phase. At $t = 0.09t_f$, there are, however, some field lines which have not yet reconnected (e.g., the remaining black and grey field lines in Figure 3f). These are examples of the field lines that are reconnected during the second phase of the reconnection. Movies S2 and S3, available in the supporting information, show the evolution of all of these field lines from side and top views throughout the reconnection experiment.

One important point to note is that the black and grey (pre-reconnection) field lines do not lie along the separator, but cross by it, entering almost parallel to the spine of the lower null and then leaving parallel to the upper null's spine. This means that the field lines twist through ≈180° about the separator before

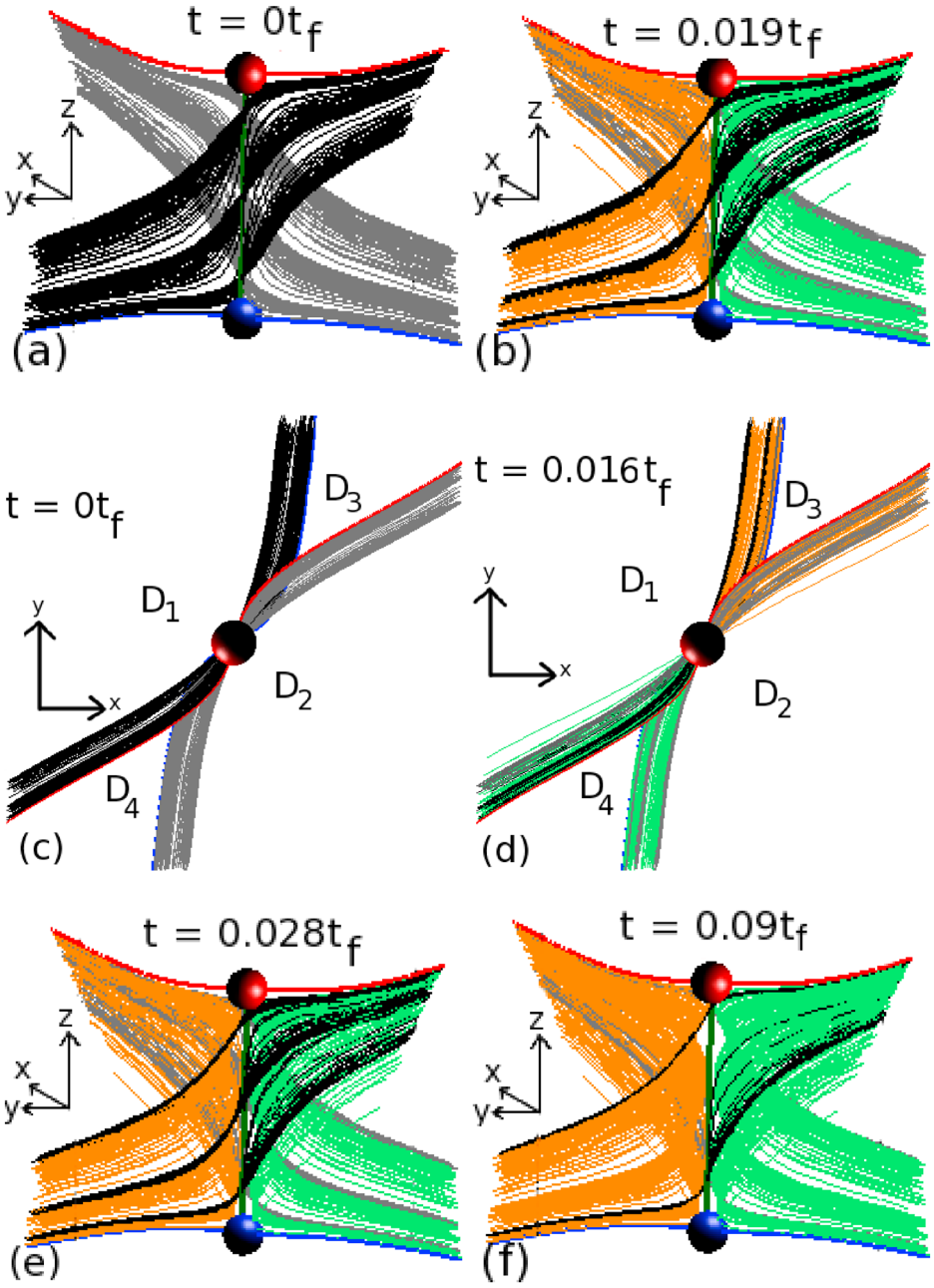

Figure 3. Positive/negative nulls (blue/red spheres) with spines (blue/red lines) and dark green separator. Black and grey field lines are drawn, at $t = 0t_f$, within the regions which lie outwith the cusps (i.e., D_1 and D_2, respectively). When the grey/black field lines reconnect, their colors change to orange/green and they lie in regions D_3/D_4, respectively. (a and c) $t = 0t_f$ (side and top views), (b and d) $t = 0.019t_f$ (side and top views), and (e) $t = 0.028t_f$ and (f) $t = 0.09t_f$.

they reconnect. After they reconnect (orange and green lines) the field lines still run almost parallel to the lower null's spine but now leave running parallel to the other side of the upper null's spine. To do this, the field lines run almost straight up the separator and barely twist around it at all.

The reconnection at the separator rapidly dissipates the current above $|\mathbf{j}| = j_{crit}$ in the MHS equilibrium current layer, which lies along the length of the separator. The current at $t = 0.09t_f$, in a cut across the separator at $z = 0.4$ (Figure 4, cf. with Figure 1b which is the same plot but in the initial equilibrium state), decreases at the separator current layer but does not decrease along the separatrix surfaces since the value of current here is less than j_{crit}. The current along the entire length of the separator diminishes quickly from its peak of 22.4 and mean of 19.5 during the first phase until it is just below the value of j_{crit} at about $|\mathbf{j}| = 9.8$ all the way

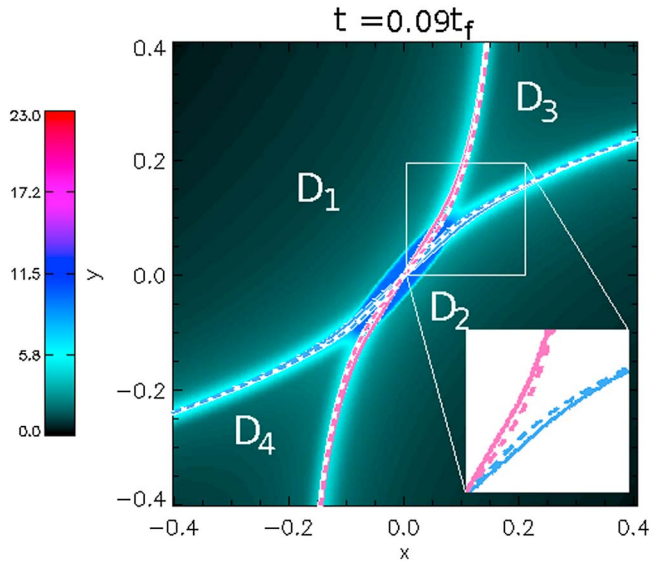

Figure 4. Contours of $|\mathbf{j}|$, in a cut at $z = 0.4$ across the separator, at $t = 0.09t_f$. The intersections of the lower (pale blue) and upper (pink) null's separatrix surfaces with this plane are also plotted at $t = 0t_f$ (dashed lines) and at $t = 0.09t_f$ (solid lines) on top of the white lines so they are distinct from the contours. The separatrix surfaces split the cut up into four regions marked as D_1, D_2, D_3, and D_4. The insert shows the separatrix surfaces of the equilibrium field and the field at $t = 0.09t_f$, in the region $0.0 \leq x, y \leq 0.2$, close-up.

along the separator. This is an indication that separator reconnection occurs along nearly the whole length of the separator and not just at one point as in null point reconnection (in agreement with *Parnell et al.* [2010a]). After the first phase, the current does not really change along the separator.

The dissipation of the current at the separator causes the separatrix surfaces of the nulls to open up slightly in the cusp regions, as flux is transferred from domains D_1 and D_2 outside the cusps to the domains D_3 and D_4 that are inside the cusps. This behavior is visible in Figure 4 where the intersections of the separatrix surfaces of both nulls with this plane are plotted at $t = 0t_f$ (dashed pale blue/pink lines) and at the same time that the contours of $|\mathbf{j}|$ are drawn, $t = 0.09t_f$ (solid pale blue/pink lines). The separatrix surfaces of the nulls are shown to open up slightly within the cusp regions (for close-up see Figure 4 insert), as a consequence of the reconnection.

The reconnection causes the nulls to move slightly apart in the z direction, with the maximum length of the separator throughout the experiment just 1.005 times greater than the equilibrium separator length. The lower null moves downward from its initial position, along the z axis, by $0.1L_0$ in the first $0.03t_f$, whereas the upper null moves upward $0.08L_0$ along the z axis, in the first $0.01t_f$. After these times both nulls move very slowly away from each other (the lower null moves a farther distance of $1 \times 10^{-4}L_0$, and the upper null moves a farther $5 \times 10^{-5}L_0$) during the rest of the experiment.

5.2. Nature of $E_\parallel$

In 3-D, a nonzero integral of $E_\parallel$ ($= \eta j_\parallel$) along a field line indicates the existence of reconnection [*Schindler et al.*, 1988; *Hornig and Schindler*, 1996]. Furthermore, in a situation where there is a single simple diffusion region, such as we have here, the maximum integral of $E_\parallel$ identifies the main reconnection site, as well as the reconnection rate [*Hesse and Birn*, 1993]. Since all the field lines that thread the nonideal region ($\eta_d \neq 0$) thread planes that cross perpendicular to the separator, we determine the integral of $E_\parallel$ along field lines that thread the plane $z = 0.4$ at $t = 0.019t_f$ during phase I. A contour plot of $\int_l E_\parallel dl$ (Figure 5) shows that the strongest reconnection occurs at the separator (in agreement with *Parnell et al.* [2010a]). The insert in this figure shows a close-up of the contours around the separator in this cut and highlights the strength of the localized peak of the integral of $E_\parallel$ along field lines at the separator. Weaker reconnection occurs on neighboring field lines creating nonzero $\int_l E_\parallel dl$ regions along the separatrix surfaces that form the separator. Now that we have confirmed that the reconnection in our experiment is separator reconnection, we look at the time evolution of various parameters along the separator to determine more details about the nature of the reconnection itself.

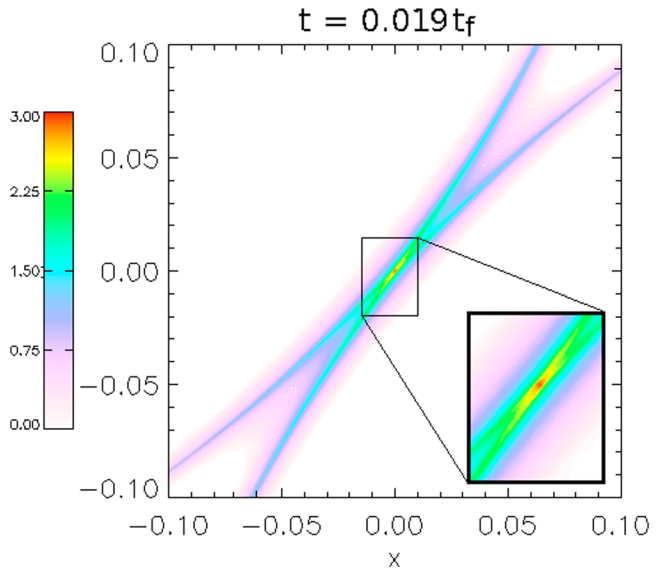

Figure 5. Contours of the integral of $E_{\parallel}$ along field lines which thread this plane perpendicular to the separator at $z=0.4$, at $t=0.019t_f$. The insert shows a close-up view of the region highlighted by the box around the separator.

Figure 6a shows how the parallel component of the electric field ($E_{\parallel}$) along the separator evolves in time as the reconnection proceeds. The separator is normalized such that it has length one for all time according to the equation $z^*=(z-z_l)/l_{sep}$ where z_l (the z coordinate of the lower null) and l_{sep} (the length of the separator) take their respective values for the frame being considered. The strongest reconnection occurs between about $z^*=0.16$ and $z^*=0.7$. Midway between these points is close to where the initial peak in current lies indicating that the peak reconnection is occurring where the current is strongest, as expected. Note that the strongest values of $E_{\parallel}$ lie midway along the separator away from the nulls indicating that the null points are not involved in separator reconnection (in agreement with *Parnell et al.* [2010a]).

After about $t = 0.03t_f$, the peak $E_{\parallel}$ (Figure 6a) is about half of what it was at the start of the experiment and decreases over the next $t = 0.06t_f$ to almost nothing. During the second phase, patches of $E_{\parallel} > 0$ are visible in Figure 6a. These regions, which have $|\mathbf{j}| \geq j_{crit}$, exist very briefly since the current in excess of j_{crit} is immediately dissipated due to the nature of the nonuniform diffusivity. Although these small reconnection events do not exist for long (compared to the reconnection in phase I), there are a significant number of these events such that the total flux reconnected slowly grows in phase II, as shown in Figure 2c.

The solid black curve in Figure 6a is the zeroth contour of the discriminant of the perpendicular component of the magnetic field ($\mathbf{B}_{\perp}$), along the separator. This contour highlights that the projected magnetic field lines are locally elliptic (O type), in planes perpendicular to the separator, in the regions where $E_{\parallel}$ is strongest, during phase I. Elsewhere in phase I, and everywhere in phase II, the projected magnetic field lines are locally hyperbolic (X type) in planes perpendicular to the separator. This behavior is consistent with that discussed in section 5.1 where the pre-reconnected field wound around the separator ≈180°, while after reconnection the field lines ran more parallel to the separator and did not cross it. This has been seen before in separator reconnection experiments by *Parnell et al.* [2010a] who found that cuts across the separator, where the reconnection was strongest, corresponded to 2-D O-type magnetic field configurations.

5.3. Behavior of the Local Reconnection Flows

Unlike in 2-D reconnection, the flows local to separator reconnection are not simple stagnation flows. *Schindler et al.* [1988], *Hesse and Schindler* [1988], and *Hornig and Schindler* [1996] have shown that in 3-D, the flow in the diffusion region counterrotates such that a continuum of field lines discontinuously reconnect at the separator in a manner that is not pairwise. This is indeed the case for separator reconnection, as evidenced by the vorticity parallel to the separator, $\omega_z = (\nabla \times \mathbf{v})_z$, (Figure 6b). Therefore, in 3-D separator reconnection the magnetic field lines undergo a rotational slippage about the separator, which is not surprising since they are effectively undoing their ≈180° twist about the separator.

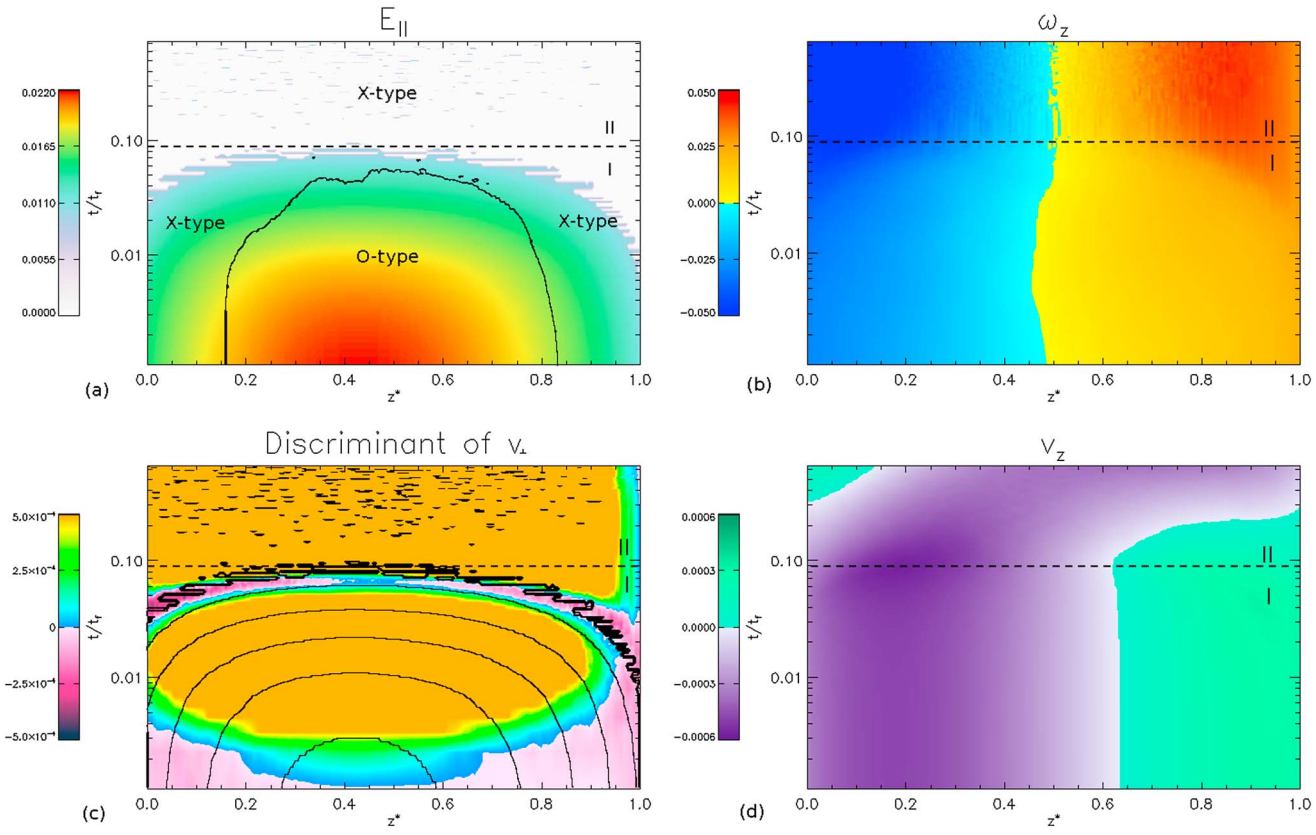

Figure 6. (a) The time evolution of $E_{\parallel}$ (colored contours) with the zeroth contour of the discriminant of $\mathbf{B}_{\perp}$ overplotted as black lines and the nature of the 2-D magnetic field lines in planes perpendicular to the separator annotated on the plot. (b) The component of the vorticity parallel to the separator ($\omega_z = (\nabla \times \mathbf{v})_z$). (c) The discriminant of $\mathbf{v}_{\perp}$ and contours of $E_{\parallel}$ (shown in Figure 6a) are overplotted as black lines. (d) The z component of the velocity, v_z, along the separator (which is normalized to lie between $z^* = 0$ and $z^* = 1$). The vertical axis on each plot is logarithmic to highlight the behavior during the first phase, and the dashed line (and symbols I and II) indicate where the first phase ends and the second phase begins.

Indeed, Figure 6b shows that the streamlines curl around the separator in opposite directions above and below a point initially around $z^* = 0.48$ (midway between where the current and pressure are initially highest on the separator). This point, about which the streamlines counterrotate, moves downward along the separator during phase I (when the value of $E_{\parallel}$ here is strong) before returning to around $z^* = 0.49$ near the end of phase I where it remains during phase II. Thus, the point on the separator about which the flow counterrotates is close to but not coincident with the position of the peak reconnection along the separator.

To discover more about the nature of the flow, we also look at the time evolution of the discriminant of the component of velocity perpendicular to the separator ($\mathbf{v}_{\perp}$) (colored contours in Figure 6c). This plot indicates that in planes perpendicular to the separator, the flow starts off O type locally about the separator, although the velocities here are very small and so there is effectively no flow. The flow perpendicular to the separator then becomes X type away from the nulls during the first phase where strong reconnection is occurring (the black lines in Figure 6c are contours of $E_{\parallel}$ along the separator, as determined in Figure 6a). As the reconnection rate during phase I decreases, the perpendicular flow once again becomes O type briefly. For the second phase, the local perpendicular flow returns to X type about the separator along almost its entire length except for very close to the upper null.

Parnell et al. [2010a] studied the local velocity flow and local magnetic field structure in planes perpendicular to a 3-D separator during separator reconnection and found a clear-cut relationship between velocity flow and magnetic field local to the separator: when the local flow is O type, the local magnetic field is X type, and vice versa. Here comparing the contours of the discriminant of $\mathbf{v}_{\perp}$ (Figure 6c) with the contours of the discriminant of $\mathbf{B}_{\perp}$, black lines in Figure 6a, we see that there is no clear correspondence between the nature of the local flow and field about the separator. At the start of the experiment, the magnetic field local to the separator is strongly O type (away from the nulls where, by definition, it must be X type), but the velocities are too small to

really claim that the flow is actually O type. The O-type magnetic field persists on the separator, and the velocity becomes X type along almost the entire length of the separator (in agreement with *Parnell et al.* [2010a]). Briefly, when $E_{\|}$ is decreasing rapidly to zero, the flow about the separator becomes O type: at this time the perpendicular magnetic field is already X type (again in agreement with *Parnell et al.* [2010a]). After this an X-type velocity flow then returns and persists throughout the weak bursty reconnection phase (phase II) where the perpendicular magnetic field local to the separator is also X type along its whole length (contrary to *Parnell et al.* [2010a]). Thus, the relationship between the local flow and field within the diffusion region is not as simple as *Parnell et al.* [2010a] state; however, during rapid reconnection the configuration does tend to involve field lines with a twist that are untwisted by a counterrotating stagnation-type flow.

We have considered the behavior of the flows into and out from the separator, but what are they like along the separator? Figure 6d shows the z component of velocity along the separator, which, for the whole of phase I, is directed outward toward the nulls from a point at $z^*=0.63$. This location is coincident neither with the location of the peak reconnection, nor with the point of counterrotation, nor with the peak pressure along the separator (which is located at about $z^*=0.57$). The point of divergence of this flow abruptly changes as phase II starts and gradually moves up to the upper null such that along the separator the flow is almost entirely downward. Toward the end of phase II, near the lower null an upflow along the separator is formed.

So except for a brief period during which the reconnection is rapidly decelerating toward the end of phase I, the local flow about the separator is essentially a form of counterrotating stagnation flow in which the field in the diffusion region is swept into the separator while rotating and then outward down toward the nulls and away from the separator, again while rotating. Due to the lack of colocation of the counterrotation point and the outflow point of flow along the separator, in the region of peak reconnection the local flows are more complicated. Note that details of the nature of the flows farther out from the separator are discussed in *Stevenson and Parnell* [2015].

Finally, the z component of the curl of **B** along the separator (not shown) decreases over time, revealing that the magnetic field relaxes as the reconnection proceeds. So the magnetic field behavior is as expected and is consistent with the field relaxing, via reconnection, from a twisted state.

6. Parameter Analysis: η_d, j_{crit}, and ν

In order to investigate the effects of (i) the anomalous diffusivity η_d, (ii) the size of the diffusion region (by changing the value of j_{crit}), and (iii) the background viscosity ν, we run additional experiments in which each of these parameters is varied in turn. The results from these runs are discussed in the sections below.

Experiments with three different values of diffusivity ($\eta_d=0.0005$, 0.001-main experiment, and 0.002) with $j_{crit}=10$ and $\nu=0.01$, then three different values of j_{crit} ($j_{crit}=10$-main experiment, $j_{crit}=7.5$, and $j_{crit}=8.5$) with $\eta=0.001$ and $\nu=0.01$, and finally three different values of ν ($\nu=0.005$, 0.01-main experiment, and 0.02) with $\eta=0.001$ and $j_{crit}=10$ are studied. None of the plasma parameters nor the initial magnetic field have changed from the original experiment in these runs except for those stated here.

6.1. Effects of Varying η_d, j_{crit}, and ν on the Reconnection Rate

First, we investigate how the reconnection rate and the total flux reconnected depend on η_d, j_{crit} and ν. As one might expect, the higher the value of η_d, the faster the reconnection, but the shorter the fast-reconnection phase (phase I) (Figure 7a). The total amount of reconnected flux in all three cases is similar but appears to marginally increase as η_d increases, except in the experiment with $\eta_d=0.002$. We believe this occurs since near the start of the experiment with the highest anomalous diffusivity ($\eta_d=0.002$) additional nulls appear in the system. These nulls, which are formed in opposite-sign pairs, appear close to the locations of the original nulls and lead to the creation of extra intercluster separators in addition to the original (intercluster) separator that linked the two original null points/null point clusters. To calculate the reconnection rate and total flux reconnected, we assume that there is just one reconnection site, the original separator. However, when there are multiple separators/reconnection sites, this assumption breaks down, and so we may not be identifying all the reconnection that occurs in the experiment with $\eta_d=0.002$. This is the only experiment discussed here which displays this behavior. The creation of these multiple nulls and separators, and the reconnection associated with them, will be studied in a follow-up paper.

From Figure 7b, we see that the smaller the diffusion region (i.e., the higher the value of j_{crit}), the shorter the fast-reconnection phase (phase I). This, of course, is expected as a smaller diffusion region contains less flux

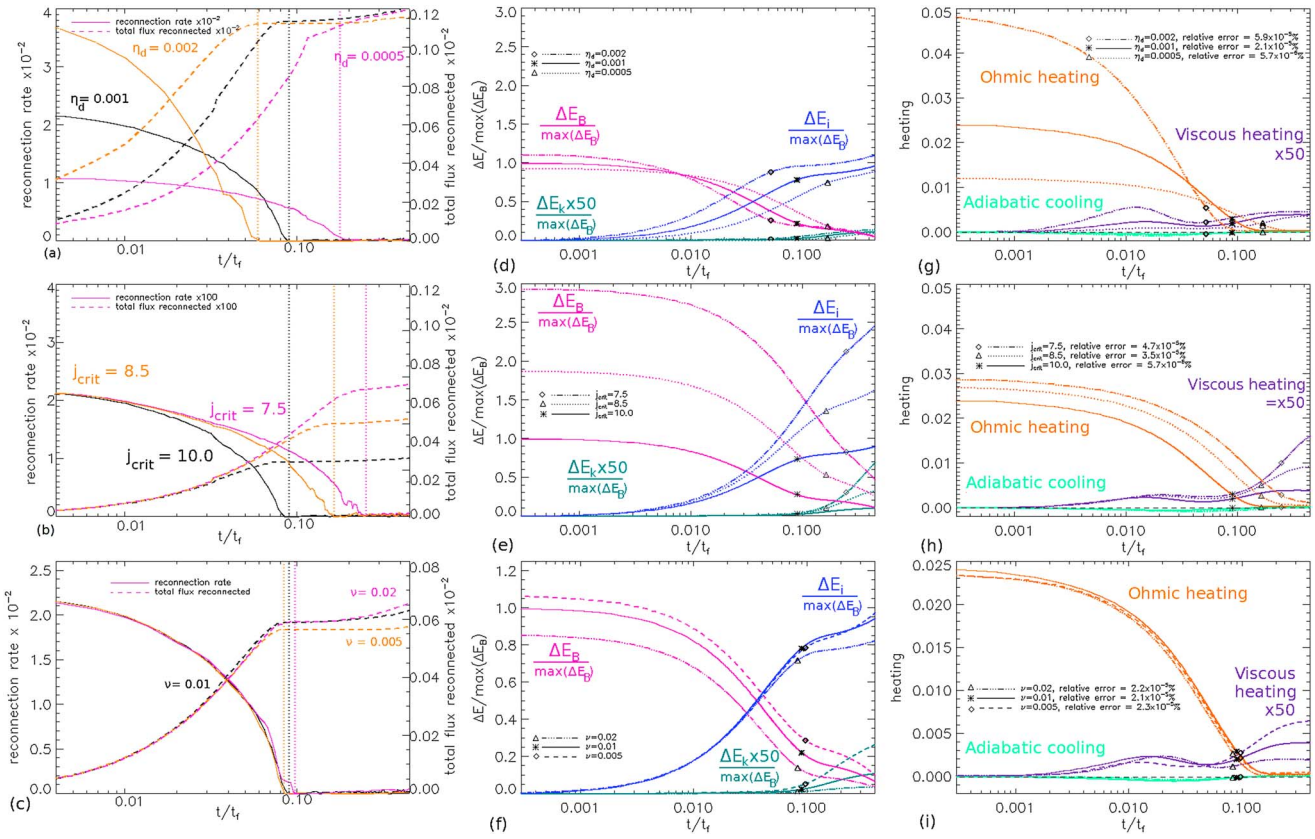

Figure 7. (a–c) The reconnection rate (solid lines) and the total flux reconnected (dashed lines), multiplied by 100; (d–f) the energy; and (g–i) the heating terms all plotted against time for experiments with $\eta_d = 0.0005$, $\eta_d = 0.001$, and $\eta_d = 0.002$ with $j_{crit} = 10$ and $\nu = 0.01$ (Figures 7a, 7d, and 7g) ; $j_{crit} = 7.5$, $j_{crit} = 8.5$, and $j_{crit} = 10$ with $\eta_d = 0.001$ and $\nu = 0.01$ (Figures 7b, 7e, and 7h); and $\nu = 0.005$, $\nu = 0.01$, and $\nu = 0.02$ with $\eta_d = 0.001$ and $j_{crit} = 10$ (Figures 7c, 7f, and 7i). In Figures 7a–7c dashed vertical lines (colored to match the respective experiment) highlight the time at which phase I ends and phase II begins for each experiment. In Figures 7d–7i symbols (annotated on the plots) indicate where phase I ends and phase II begins.

to reconnect. However, the peak reconnection rate is unaffected by the value of j_{crit}. Thus, the total amount of flux reconnected increases as j_{crit} is lowered.

From Figure 7c, we find that varying the value of ν has little effect on the reconnection rate during the fast-reconnection phase. During phase II a smaller viscosity is associated with a marginally faster reconnection rate. This is because the resulting flows that drive the steady state reconnection of phase II are stronger in a fluid that is less viscous. This leads to more flux being reconnected overall in the case with the lowest viscosity.

6.2. Effects of Varying Diffusivity η_d on the Energetics

For the three experiments with varying η_d, the same basic behavior of energies is found as that seen in the main experiment (Figures 7d and 7g). The change in energies is normalized to the maximum change in the magnetic energy of the main experiment (where $\eta_d = 0.001$, $j_{crit} = 10$, and $\nu = 0.01$) so that the energy release of all experiments can be compared. As before, most of the magnetic energy lost is converted directly into internal energy with only a little kinetic energy (multiplied by 50 for representational purposes) generated (Figure 7d). Varying η_d leads to a change in the rate of loss of magnetic energy: naturally, the experiment with the highest η_d experiences the most rapid loss, but the shortest fast-reconnection phase (phase I). The total loss of magnetic energy increases as η_d increases.

Most of the additional energy comes directly from Ohmic heating. A small contribution comes from viscous heating (multiplied by 50 for representational purposes), due to some wave damping occurring predominantly during phase II of each experiment (Figure 7g). The rate of viscous heating is very similar in all three experiments suggesting that the more rapid reconnection has not led to the creation of larger perturbations. In each experiment, a small amount of adiabatic cooling occurs in the later part of phase I. This occurs due to the sudden expansion of the field about the separator current layer.

From Figure 7g, it appears that the peak Ohmic heating rate is basically linearly proportional to η_d, as is the duration of phase I. However, the duration of the main Ohmic heating period (which, as shown in section 4, is slightly longer than phase I) does not vary in the same way and is shorter for large η_d than expected from a linear falloff. The relative error in the total energy is small and of the same order for all three experiments.

6.3. Effects of Varying j_{crit} on the Energetics

Here we consider the experiments with varying j_{crit}. From Figure 7e, we see that having a lower value of j_{crit} means that the total loss in magnetic energy increases and it takes longer for the majority of the magnetic energy to be converted into internal and kinetic energy. Furthermore, the kinetic energy is greater as j_{crit} decreases. These differences are not surprising, since a lower j_{crit} creates a larger diffusion region in which more current can be dissipated and creates a greater loss in force balance of the system. We find that the free energy released (calculated as a percentage of the energy released if a uniform background diffusivity was used) increases as j_{crit} decreases, with 3% of the free energy released when $j_{crit} = 10$, 5% when $j_{crit} = 8.5$, and 8% when $j_{crit} = 7.5$.

In Figure 7h, it is no surprise to see that the initial amount of Ohmic heating increases as j_{crit} decreases. Additionally, a lower initial j_{crit} leads to greater viscous heating associated with the larger kinetic energies in the system.

6.4. Effects of Varying ν on the Energetics

Varying the value of the background viscosity, ν, has little effect on the total loss in magnetic energy (Figure 7f). This is reflected in the Ohmic dissipation (Figure 7i), which appears to be basically the same in all experiments. The proportion of magnetic energy converted to kinetic energy during the experiment does depend on viscosity with a larger ν, corresponding to greater viscous heating in phase I, leading to smaller kinetic energy since the waves are damped to a greater extent. This means that near the end of phase I, and throughout phase II, the kinetic energy is greatest for experiments with lower ν. In phase II, we find that the larger the ν, the weaker the Ohmic heating. The adiabatic cooling term appears to be unaffected by the size of the viscosity.

7. Conclusions

In this paper, we have studied the properties of spontaneous (undriven) reconnection at a 3-D separator current layer using a resistive MHD code. We start from a system containing free energy, which is in MHS equilibrium everywhere save for very small forces at the current enhancements about the separator and separatrix surfaces: a perfect equilibrium would take an infinite time to form [*Stevenson et al.*, 2015]. An anomalous diffusivity, η_d, is used to mimic the onset of microinstabilities, which only acts where the current is greater than a set amount, j_{crit}, such that reconnection only occurs at the separator current layer and, for low enough j_{crit}, a little way along the separatrix surfaces.

In our experiments, unlike driven separator reconnection experiments, such as *Haynes et al.* [2007] and *Parnell et al.* [2010a], the reconnection starts immediately and its rate is dictated simply by the value of the anomalous diffusivity and is not influenced by an external driver. We find that the reconnection occurs in two distinct phases: a short fast-reconnection phase followed by a longer slow impulsive bursty reconnection phase. Such a partitioning into distinct phases is the same as that found in 2-D spontaneous reconnection experiments at null points [e.g., *Fuentes-Fernández et al.*, 2012a, 2012b], but here an impulsive bursty regime is found even at high beta.

In the main experiment, where $\eta_d = 0.001$, $j_{crit} = 10$, and $\nu = 0.01$, most (88%) of the reconnection occurs during the first short phase that lasts just $0.09t_f$, in which the current is rapidly dissipated away from the current layer. During this phase magnetic energy is mainly (99.77%) converted directly into internal energy via Ohmic dissipation. Only a small amount (0.23%) of energy is converted from magnetic to kinetic energy during this phase and then transferred into internal energy via viscous damping. Additionally, due to a rapid expansion of the plasma as a result of the sudden reconnection, a small amount of adiabatic cooling is observed during phase I. Even during the slow impulsive bursty reconnection phase, the limited Ohmic heating dominates over the viscous heating. This is likely to be a consequence of the high-beta plasma within which the separator is embedded since, in such a plasma, as a current layer is formed, a strong pressure gradient force rapidly develops balancing the Lorentz force making it harder for strong current layers to form than in the equivalent low-beta system. Consequently at a high-beta separator current layer, the perturbation caused by the sudden onset of reconnection will be smaller than in the low-beta case. Furthermore, the combination

of a smaller perturbation and denser plasma in the high-beta, as opposed to low-beta, system means that little plasma is accelerated and, hence, a low kinetic energy is found. Further studies are needed to establish under what conditions, if any, a low-beta regime produces greater viscous heating than Ohmic heating.

Although the kinetic energy is relatively small, this in no way implies that waves and flows are not produced. The rapid loss of equilibrium caused as a result of the reconnection in the separator current layer naturally launches waves that generate flows within the system. These waves and flows are discussed in detail in the second paper of this series [*Stevenson and Parnell*, 2015].

The rate of reconnection in the first phase is up to 22 times faster than in the second phase, and the maximum reconnection rate increases as η_d gets larger. However, the duration of the first phase shortens as η_d increases, such that the total amount of flux reconnected in this phase is independent of η_d. As j_{crit} increases, the length of the first phase also decreases, but here the total amount of flux reconnected in the first phase increases as j_{crit} decreases. Varying the value of the background viscosity has little effect on both the rate of reconnection and the length of the first phase.

In this paper, the reconnection rates we quote are dimensionless. These rates may be scaled to dimensional values by multiplying by $B_n L_n^2/t_n$, where B_n (*T*), L_n (m) and t_n (s) are the normalizing magnetic field, length, and time. For example, numerical modeling of separator reconnection at the dayside magnetopause by *Komar et al.* [2013] and *Komar* [2015] found separators of length L_n=223 Mm within magnetic fields with strengths B_n=5 nT. Applying these values, with a time scale of t_n=1 s, we find that the peak reconnection rate at the start of our main experiment is 5.6×10^6 V. This value is over 100 times greater than the observed value found by *Chisham et al.* [2004] who looked at high-latitude dayside reconnection with northward IMF. Our values better match with those found by *Pinnock et al.* [2003] (which range from 1.1×10^6 V to 9×10^6 V) who found the rate of reconnection along the projection of a separator in the ionosphere.

Similarly, our diffusivity ($\eta_d = 0.001$) can be scaled to dimensional values in the dayside magnetopause by multiplying by $L_n v_{A_n}/R_m$, where v_{An} is the Alfvén speed scaling factor. *Komar* [2015] found Alfvén speeds of 380 km s^{-1}; hence, our diffusivity $\eta_d = L_n v_{An}/R_m = 8.5\times10^{10}$ m^2 s^{-1} (where $R_m = 10^3$ as discussed in section 3). This value is comparable with that used in *Komar et al.* [2013] ($\eta_K = 6\times10^{10}$ m^2 s^{-1}) who studied similar experiments to those detailed in *Komar* [2015].

During phase I, the strength of the reconnection, which occurs asymmetrically along the entire length of the separator with the strongest reconnection occurring away from the null points, decreases and only weak, short-lived reconnection events occur in phase II. During this second phase, the impulsive bursts of reconnection occur randomly in small localized regions on the separator away from its ends. Each event is very weak and short lived. These events do not start until $t = 0.17t_f$, some $0.08t_f$ after the end of the first phase. During this time we suspect that the system is again trying to regain equilibrium and so builds up the current along the separator. The instant the current anywhere along the separator rises above j_{crit}, a little burst of reconnection dissipates it.

We have found that regions along the separator where the reconnection is strongest are associated with O-type perpendicular magnetic field lines local to the separator and that regions where the reconnection is weaker, in phase I, and throughout all of phase II, are associated with perpendicular magnetic field that is locally X type. Note that the signature of O-type field actually comes from field lines that twist through just 180° as they run up the separator. On the other hand, the X type arises because the newly reconnected field lines slightly twist back on themselves as they run up the separator. Therefore, identifying a separator or separator reconnection from knowledge of the local magnetic field behavior is not possible, as mentioned in section 1: separators are global features, and therefore, knowledge of the global field is required to locate them. However, since strong 3-D reconnection is associated with a parallel electric field and, hence, (under the conditions of a classical Ohm's law) is associated with a parallel electric current, magnetic fields that locally have an O-type nature in planes perpendicular to them are potential sites for reconnection.

A counterrotating flow also exists at a point along the separator close to, but not coincident with, the peak reconnection. This counterrotation of the flow exists simultaneously with both O-type and X-type flows local to the separator. Indeed, the strongest reconnection appears to be associated with a counterrotating stagnation flow about the separator with the reconnected field moving outward toward the nulls and away from the separator. The system starts with very weak flow which appears initially to be elliptic perpendicular to

the separator, but then turns to a stagnation-type flow, suggesting that the stagnation flow is generated as a result of the reconnection.

In a companion paper [*Stevenson and Parnell*, 2015], we discuss the properties of the waves which are launched from the diffusion site as a consequence of the loss of force balance due to the reconnection. The flows which these waves set up are also discussed in detail.

Acknowledgments
J.E.H.S. undertook much of this work during her PhD during which she was supported financially by STFC. J.E.H.S. is now a postdoc in the SMTG in St. Andrews funded on their STFC consolidated grant. The computations for this paper were carried out on the St. Andrews's UKMHD consortium cluster which is funded by STFC and SRIF. Data from simulation results are available on request from J.E.H. Stevenson (e-mail: jm686@st-andrews.ac.uk).

References

Arber, T. D., A. W. Longbottom, C. L. Gerrard, and A. M. Milne (2001), A staggered grid, Lagrangian-Eulerian remap code for 3-D MHD simulations, *J. Comput. Phys.*, *171*, 151–181, doi:10.1006/jcph.2001.6780.

Aulanier, G., E. Pariat, and P. Démoulin (2005), Current sheet formation in quasi-separatrix layers and hyperbolic flux tubes, *Astron. Astrophys.*, *444*, 961–976, doi:10.1051/0004-6361:20053600.

Aulanier, G., E. Pariat, P. Démoulin, and C. R. DeVore (2006), Slip-running reconnection in quasi-separatrix layers, *Sol. Phys.*, *238*, 347–376, doi:10.1007/s11207-006-0230-2.

Bareford, M. R., A. W. Hood, and P. K. Browning (2013), Coronal heating by the partial relaxation of twisted loops, *Astron. Astrophys.*, *550*, A40, doi:10.1051/0004-6361/201219725.

Barnes, G., D. W. Longcope, and K. D. Leka (2005), Implementing a magnetic charge topology model for solar active regions, *Astrophys. J.*, *629*, 561–571, doi:10.1086/431175.

Browning, P. K., C. Gerrard, A. W. Hood, R. Kevis, and R. A. M. van der Linden (2008), Heating the corona by nanoflares: Simulations of energy release triggered by a kink instability, *Astron. Astrophys.*, *485*, 837–848, doi:10.1051/0004-6361:20079192.

Chisham, G., M. Freeman, I. Coleman, M. Pinnock, M. Hairston, M. Lester, and G. Sofko (2004), Measuring the dayside reconnection rate during an interval of due northward interplanetary magnetic field, *Ann. Geophys.*, *22*, 4243–4258, doi:10.5194/angeo-22-4243-2004.

Close, R. M., C. E. Parnell, and E. R. Priest (2004), Separators in 3D quiet-Sun magnetic fields, *Sol. Phys.*, *225*, 21–46, doi:10.1007/s11207-004-3259-0.

Close, R. M., C. E. Parnell, D. W. Longcope, and E. R. Priest (2005), Coronal flux recycling times, *Sol. Phys.*, *231*, 45–70, doi:10.1007/s11207-005-6878-1.

Cnossen, I., M. Wiltberger, and J. E. Ouellette (2012), The effects of seasonal and diurnal variations in the Earth's magnetic dipole orientation on solar wind-magnetosphere-ionosphere coupling, *J. Geophys. Res.*, *117*, A11211, doi:10.1029/2012JA017825.

Craig, I. J. D., R. B. Fabling, S. M. Henton, and G. J. Rickard (1995), An exact solution for steady state magnetic reconnection in three dimensions, *Astrophys. J. Lett.*, *455*, L197, doi:10.1086/309822.

De Moortel, I., and K. Galsgaard (2006a), Numerical modelling of 3D reconnection due to rotational footpoint motions, *Astron. Astrophys.*, *451*, 1101–1115, doi:10.1051/0004-6361:20054587.

De Moortel, I., and K. Galsgaard (2006b), Numerical modelling of 3D reconnection: II. Comparison between rotational and spinning footpoint motions, *Astron. Astrophys.*, *459*, 627–639.

Demoulin, P., J. C. Henoux, E. R. Priest, and C. H. Mandrini (1996), Quasi-separatrix layers in solar flares: I. Method, *Astron. Astrophys.*, *308*, 643–655.

Demoulin, P., L. G. Bagala, C. H. Mandrini, J. C. Henoux, and M. G. Rovira (1997), Quasi-separatrix layers in solar flares: II. Observed magnetic configurations, *Astron. Astrophys.*, *325*, 305–317.

Deng, X. H., et al. (2009), Dynamics and waves near multiple magnetic null points in reconnection diffusion region, *J. Geophys. Res.*, *114*, A07216, doi:10.1029/2008JA013197.

Dorelli, J. C., and A. Bhattacharjee (2008), Defining and identifying three-dimensional magnetic reconnection in resistive magnetohydrodynamic simulations of Earth's magnetosphere, *Physics of Plasmas*, *15*(5), 056504, doi:10.1063/1.2913548.

Dorelli, J. C., and A. Bhattacharjee (2009), On the generation and topology of flux transfer events, *J. Geophys. Res.*, *114*, A06213, doi:10.1029/2008JA013410.

Dorelli, J. C., A. Bhattacharjee, and J. Raeder (2007), Separator reconnection at Earth's dayside magnetopause under generic northward interplanetary magnetic field conditions, *J. Geophys. Res.*, *112*, A02202, doi:10.1029/2006JA011877.

Edwards, S. J., and C. E. Parnell (2015), Null point distribution in global coronal potential fields, *Sol. Phys.*, *290*, 2055–2076.

Edwards, S. J., C. E. Parnell, L. K. Harra, J. L. Culhane, and D. H. Brooks (2015), A comparison of global magnetic field skeletons and active-region upflows, *Sol. Phys.*, 1–26, doi:10.1007/s11207-015-0807-8.

Evans, C. R., and J. F. Hawley (1988), Simulation of magnetohydrodynamic flows—A constrained transport method, *Astrophys. J.*, *332*, 659–677, doi:10.1086/166684.

Fuentes-Fernández, J., C. E. Parnell, A. W. Hood, E. R. Priest, and D. W. Longcope (2012a), Consequences of spontaneous reconnection at a two-dimensional non-force-free current layer, *Phys. Plasmas*, *19*(2), 022901, doi:10.1063/1.3683002.

Fuentes-Fernández, J., C. E. Parnell, and E. R. Priest (2012b), The onset of impulsive bursty reconnection at a two-dimensional current layer, *Phys. Plasmas*, *19*(7), 072901, doi:10.1063/1.4729334.

Galsgaard, K., and Å. Nordlund (1996), Heating and activity of the solar corona: 1. Boundary shearing of an initially homogeneous magnetic field, *J. Geophys. Res.*, *101*, 13,445–13,460, doi:10.1029/96JA00428.

Galsgaard, K., and Å. Nordlund (1997a), Heating and activity of the solar corona: 2. Kink instability in a flux tube, *J. Geophys. Res.*, *102*, 219–230, doi:10.1029/96JA01462.

Galsgaard, K., and Å. Nordlund (1997b), Heating and activity of the solar corona: 3. Dynamics of a low beta plasma with three-dimensional null points, *J. Geophys. Res.*, *102*, 231–248, doi:10.1029/96JA02680.

Galsgaard, K., and C. E. Parnell (2005), Elementary heating events-magnetic interactions between two flux sources: III. Energy considerations, *Astron. Astrophys.*, *439*, 335–349, doi:10.1051/0004-6361:20052775.

Galsgaard, K., E. R. Priest, and Å. Nordlund (2000), Three-dimensional separator reconnection—How does it occur?, *Sol. Phys.*, *193*, 1–16, doi:10.1023/A:1005248811680.

Guo, R., et al. (2013), Separator reconnection with antiparallel/component features observed in magnetotail plasmas, *J. Geophys. Res. Space Physics*, *118*, 6116–6126, doi:10.1002/jgra.50569.

Haynes, A. L. (2008), Magnetic skeletons and 3D magnetic reconnection, PhD thesis, School of Math. and Stat., Univ. of St Andrews, St Andrews, Scotland.

Haynes, A. L., and C. E. Parnell (2007), A trilinear method for finding null points in a three-dimensional vector space, *Phys. Plasmas*, *14*(8), 082107, doi:10.1063/1.2756751.

Haynes, A. L., and C. E. Parnell (2010), A method for finding three-dimensional magnetic skeletons, *Phys. Plasmas*, *17*(9), 092903, doi:10.1063/1.3467499.
Haynes, A. L., C. E. Parnell, K. Galsgaard, and E. R. Priest (2007), Magnetohydrodynamic evolution of magnetic skeletons, *Proc. R. Soc. A*, *463*, 1097–1115, doi:10.1098/rspa.2007.1815.
Hesse, M., and J. Birn (1993), Parallel electric fields as acceleration mechanisms in three-dimensional magnetic reconnection, *Adv. Space Res.*, *13*, 249–252, doi:10.1016/0273-1177(93)90341-8.
Hesse, M., and K. Schindler (1988), A theoretical foundation of general magnetic reconnection, *J. Geophys. Res.*, *93*, 5559–5567, doi:10.1029/JA093iA06p05559.
Hood, A. W., P. K. Browning, and R. A. M. van der Linden (2009), Coronal heating by magnetic reconnection in loops with zero net current, *Astron. Astrophys.*, *506*, 913–925, doi:10.1051/0004-6361/200912285.
Hornig, G., and K. Schindler (1996), Magnetic topology and the problem of its invariant definition, *Phys. Plasmas*, *3*, 781–791, doi:10.1063/1.871778.
Hu, S., A. Bhattacharjee, J. Dorelli, and J. M. Greene (2004), The spherical tearing mode, *Geophys. Res. Lett.*, *31*, L19806, doi:10.1029/2004GL020977.
Hu, Y. Q., Z. Peng, C. Wang, and J. R. Kan (2009), Magnetic merging line and reconnection voltage versus IMF clock angle: Results from global MHD simulations, *J. Geophys. Res.*, *114*, A08220, doi:10.1029/2009JA014118.
Komar, C. M. (2015), The nature of magnetic reconnection at the dayside magnetopause, PhD thesis, Eberly College of Arts and Sci., West Virginia Univ., Morgantown.
Komar, C. M., P. A. Cassak, J. C. Dorelli, A. Glocer, and M. M. Kuznetsova (2013), Tracing magnetic separators and their dependence on IMF clock angle in global magnetospheric simulations, *J. Geophys. Res. Space Physics*, *118*, 4998–5007, doi:10.1002/jgra.50479.
Laitinen, T. V., P. Janhunen, T. I. Pulkkinen, M. Palmroth, and H. E. J. Koskinen (2006), On the characterization of magnetic reconnection in global MHD simulations, *Ann. Geophys.*, *24*, 3059–3069, doi:10.5194/angeo-24-3059-2006.
Laitinen, T. V., M. Palmroth, T. I. Pulkkinen, P. Janhunen, and H. E. J. Koskinen (2007), Continuous reconnection line and pressure-dependent energy conversion on the magnetopause in a global MHD model, *J. Geophys. Res.*, *112*, A11201, doi:10.1029/2007JA012352.
Lau, Y.-T., and J. M. Finn (1990), Three-dimensional kinematic reconnection in the presence of field nulls and closed field lines, *Astrophys. J.*, *350*, 672–691, doi:10.1086/168419.
Longcope, D. W. (2001), Separator current sheets: Generic features in minimum-energy magnetic fields subject to flux constraints, *Phys. Plasmas*, *8*, 5277–5290, doi:10.1063/1.1418431.
Longcope, D. W., and S. C. Cowley (1996), Current sheet formation along three-dimensional magnetic separators, *Phys. Plasmas*, *3*, 2885–2897, doi:10.1063/1.871627.
Longcope, D. W., and C. E. Parnell (2009), The number of magnetic null points in the quiet Sun corona, *Sol. Phys.*, *254*, 51–75, doi:10.1007/s11207-008-9281-x.
Longcope, D. W., and E. R. Priest (2007), Fast magnetosonic waves launched by transient, current sheet reconnection, *Phys. Plasmas*, *14*(12), 122905, doi:10.1063/1.2823023.
Longcope, D. W., and L. Tarr (2012), The role of fast magnetosonic waves in the release and conversion via reconnection of energy stored by a current sheet, *Astrophys. J.*, *756*, 192, doi:10.1088/0004-637X/756/2/192.
Longcope, D. W., D. E. McKenzie, J. Cirtain, and J. Scott (2005), Observations of separator reconnection to an emerging active region, *Astrophys. J.*, *630*, 596–614, doi:10.1086/432039.
MacTaggart, D., and A. L. Haynes (2014), On magnetic reconnection and flux rope topology in solar flux emergence, *Mon. Not. R. Astron. Soc.*, *438*, 1500–1506, doi:10.1093/mnras/stt2285.
Masson, S., E. Pariat, G. Aulanier, and C. J. Schrijver (2009), The nature of flare ribbons in coronal null-point topology, *Astrophys. J.*, *700*, 559–578, doi:10.1088/0004-637X/700/1/559.
Ouellette, J. E., B. N. Rogers, M. Wiltberger, and J. G. Lyon (2010), Magnetic reconnection at the dayside magnetopause in global Lyon-Fedder-Mobarry simulations, *J. Geophys. Res.*, *115*, A08222, doi:10.1029/2009JA014886.
Parnell, C. E., A. L. Haynes, and K. Galsgaard (2008), Recursive reconnection and magnetic skeletons, *Astrophys. J.*, *675*, 1656–1665, doi:10.1086/527532.
Parnell, C. E., A. L. Haynes, and K. Galsgaard (2010a), Structure of magnetic separators and separator reconnection, *J. Geophys. Res.*, *115*, A02102, doi:10.1029/2009JA014557.
Parnell, C. E., R. C. Maclean, and A. L. Haynes (2010b), The detection of numerous magnetic separators in a three-dimensional magnetohydrodynamic model of solar emerging flux, *Astrophys. J. Lett.*, *725*, L214–L218, doi:10.1088/2041-8205/725/2/L214.
Peng, Z., C. Wang, and Y. Q. Hu (2010), Role of IMF B_x in the solar wind-magnetosphere-ionosphere coupling, *J. Geophys. Res.*, *115*, A08224, doi:10.1029/2010JA015454.
Phan, T. D., et al. (2006), A magnetic reconnection X-line extending more than 390 Earth radii in the solar wind, *Nature*, *439*, 175–178, doi:10.1038/nature04393.
Pinnock, M., G. Chisham, I. J. Coleman, M. P. Freeman, M. Hairston, and J.-P. Villain (2003), The location and rate of dayside reconnection during an interval of southward interplanetary magnetic field, *Ann. Geophys.*, *21*, 1467–1482, doi:10.5194/angeo-21-1467-2003.
Platten, S. J., C. E. Parnell, A. L. Haynes, E. R. Priest, and D. H. Mackay (2014), The solar cycle variation of topological structures in the global solar corona, *Astron. Astrophys.*, *565*, A44, doi:10.1051/0004-6361/201323048.
Pontin, D. I., and I. J. D. Craig (2006), Dynamic three-dimensional reconnection in a separator geometry with two null points, *Astrophys. J.*, *642*, 568–578, doi:10.1086/500725.
Pontin, D. I., and K. Galsgaard (2007), Current amplification and magnetic reconnection at a three-dimensional null point: Physical characteristics, *J. Geophys. Res.*, *112*, A03103, doi:10.1029/2006JA011848.
Pontin, D. I., G. Hornig, and E. R. Priest (2004), Kinematic reconnection at a magnetic null point: Spine-aligned current, *Geophys. Astrophys. Fluid Dyn.*, *98*, 407–428.
Pontin, D. I., G. Hornig, and E. R. Priest (2005), Kinematic reconnection at a magnetic null point: Fan-aligned current, *Geophys. Astrophys. Fluid Dyn.*, *99*, 77–93.
Pontin, D. I., A. K. Al-Hachami, and K. Galsgaard (2011), Generalised models for torsional spine and fan magnetic reconnection, *Astron. Astrophys.*, *533*, A78.
Priest, E. R., and P. Démoulin (1995), Three-dimensional magnetic reconnection without null points: 1. Basic theory of magnetic flipping, *J. Geophys. Res.*, *100*, 23,443–23,464, doi:10.1029/95JA02740.
Priest, E. R., and D. I. Pontin (2009), Three-dimensional null point regimes, *Phys. Plasmas*, *16*, 122101.
Priest, E. R., and V. S. Titov (1996), Magnetic reconnection at three-dimensional null points, *Philos. Trans. R. Soc. A*, *354*, 2951–2992, doi:10.1098/rsta.1996.0136.

Pulkkinen, T. I., M. Palmroth, H. E. J. Koskinen, T. V. Laitinen, C. C. Goodrich, V. G. Merkin, and J. G. Lyon (2010), Magnetospheric modes and solar wind energy coupling efficiency, *J. Geophys. Res.*, *115*, A03207, doi:10.1029/2009JA014737.

Régnier, S., C. E. Parnell, and A. L. Haynes (2008), A new view of quiet-Sun topology from Hinode/SOT, *Astron. Astrophys.*, *484*, L47–L50, doi:10.1051/0004-6361:200809826.

Schindler, K., M. Hesse, and J. Birn (1988), General magnetic reconnection, parallel electric fields, and helicity, *J. Geophys. Res.*, *93*, 5547–5557, doi:10.1029/JA093iA06p05547.

Sonnerup, B. U. Ö. (1979), *Magnetic Field Reconnection*, pp. 45–108, North-Holland, Amsterdam.

Stevenson, J. E. H., and C. E. Parnell (2015), Spontaneous reconnection at a separator current layer: 2. Nature of the waves and flows, *J. Geophys. Res. Space Physics*, *120*, doi:10.1002/2015JA021736.

Stevenson, J. E. H., C. E. Parnell, E. R. Priest, and A. L. Haynes (2015), The nature of separator current layers in MHS equilibria: I. Current parallel to the separator, *Astron. Astrophys.*, *573*, A44, doi:10.1051/0004-6361/201424348.

Titov, V. S., E. R. Priest, and P. Demoulin (1993), Conditions for the appearance of "bald patches" at the solar surface, *Astron. Astrophys.*, *276*, 564.

Trenchi, L., M. F. Marcucci, G. Pallocchia, G. Consolini, M. B. Bavassano Cattaneo, A. M. di Lellis, H. RèMe, L. Kistler, C. M. Carr, and J. B. Cao (2008), Occurrence of reconnection jets at the dayside magnetopause: Double Star observations, *J. Geophys. Res.*, *113*, A07S10, doi:10.1029/2007JA012774.

Wilmot-Smith, A. L., and I. De Moortel (2007), Magnetic reconnection in flux-tubes undergoing spinning footpoint motions, *Astron. Astrophys.*, *473*, 615–623, doi:10.1051/0004-6361:20077455.

Wilmot-Smith, A. L., and G. Hornig (2011), A time-dependent model for magnetic reconnection in the presence of a separator, *Astrophys. J.*, *740*, 89, doi:10.1088/0004-637X/740/2/89.

Xiao, C. J., et al. (2007), Satellite observations of separator-line geometry of three-dimensional magnetic reconnection, *Nat. Phys.*, *3*, 609–613, doi:10.1038/nphys650.